A nano-plasmonic HMIM waveguide based concurrent dual-band BPF using circular ring resonator

Miriyala Sridhar[1]*, Surendra Kumar Bitra[2], T S N Murthy[3], and Koppireddi Padmaraju[4]

1. Department of Electronics and Communication Engineering, Koneru Lakshmaiah Education Foundation, Guntur, India

2. Astra Microwave Products Ltd., Hyderabad, India

3. Department of Electronics and Communication Engineering, JNTU-GV College of Engineering, Vizianagaram, India

4. Department of Electronics and Communication Engineering, Jawaharlal Nehru Technological University Kakinada, Kakinada, India

(Received 13 July 2023; Revised 21 September 2023)

This article analyzes the transmission line characteristics of plasmonic hybrid metal insulator metal (HMIM) waveguide, circular ring resonator (CRR) based dual-band band-pass filters with two transmission poles in both pass-bands in the optical regime using coupled line feed. The transmission line characteristics of an HMIM waveguide, such as characteristic impedance (Z_{PV}), effective refractive index (n_{eff}) and propagation length (L_{spp}), have been obtained by using full wave simulation. Using basic HMIM slot waveguide, a CRR with periodic loading of double- and triple-ring CRR is numerically analyzed. Two input ports have been used for excitation, which are located at the separation of 180° positions along the CRR, and are coupled with the ring by parallel coupled lines, producing the dual pass-bands with the synchronous excitation of two transmission poles. The proposed double-ring dual-band band-pass filter (DR-DB-BPF) offers 35 dB extinction ratio (*ER*), 299.69 nm free spectral range (*FSR*) and narrow band full width half maximum (*FWHM*) of 78.057—112.43 nm. The triple-ring DB-BPF (TR-DB-BPF) has 22.5 dB *ER*, *FSR* of 292.18 nm and *FWHM* of 42.751—59.58 nm. The proposed filters are very useful in the development of dual-band filters for electronic photonic integrated circuits (EPICs), as the optical signals are filtered at two wavelengths simultaneously.

Document code: A **Article ID:** 1673-1905(2024)03-0152-5

DOI https://doi.org/10.1007/s11801-024-3130-5

Hybrid metal insulator metal (HMIM) plasmonic waveguide is currently fascinated considerably in high density electronic photonic integrated circuits (EPICs) due to their confinement outside the diffraction limit[1]. Along with various nanoplasmonic waveguides, HMIM waveguides contain the properties like simple fabrication, strong field strength, as well as comparatively lower propagation and bending losses[2-6]. Several HMIM waveguide devices like 90° bends, couplers, Y-splitter and ring resonators (RRs) at 1 550 nm are analyzed theoretically[7-11]. The RRs are indispensable components in the nanoscale communication systems. The HMIM based optical logic gates are investigated at 1 550 nm with a confinement area of 0.25 μm×0.04 μm[12]. A very limited work is carried out in HMIM based dual-band filters in the previous literature. The proposed HMIM (Ag-SiO_2-Si-SiO_2-Ag) waveguide based plasmonic devices consist of two metal claddings and an insulator of high and low dielectrics, which can confine the incident light in the dielectric region as shown in Fig.1. The SiO_2 material is used as substrate. The HMIM waveguide provides a longer propagation distance compared to the metal insulator metal (MIM) and hybrid metal insulator (HMI) waveguide with the similar optical mode confinement[5,11,12]. The band-pass filter (BPF) with multi-channel operation using coupled arrow shape is analyzed[13]. The HMIM waveguide-based coupler and waveguide with triangular grooves are investigated[14,15]. A circular ring resonator (CRR) of single section is designed and investigated for dual-band BPF applications[16]. In this work, we propose the HMIM based dual-ring dual-band BPF (DR-DB-BPF) and triple-ring dual-band BPF (TR-DB-BPF) for operating in O and L bands. All the simulations are carried out using the finite differential time domain (FDTD) solver of CST studio suite.

The mesh sizes are taken as 4 nm×4 nm. To obtain accurate results, perfect matched layer (PML) boundary conditions are used. The plasmonic filters and CRRs are crucial structural components in the wavelength-selective devices due to their regularity, simplicity and ease of fabrication. The HMIM waveguide and CRR

* E-mail: sridhar.m@kluniversity.in

structures are fabricated easily using CMOS technology[2,17]. More than three decades ago, WOLFF's research revealed the coexistence of two degenerate modes within two resonant frequency ranges[18]. Typically, these two modes are separated by manipulating the similarity of an RR to ensure excitation of the two transmission poles within the primary passband. To address the growing demand driven by the advancement of multi-functional wireless systems, there is a need for multiple dual-band BPFs. Specifically, dual-mode RR, which relies on dual-band filters, has garnered significant attention recently due to its compact size and improved performance[19-24]. One approach that attempted to exploit this specific characteristic was the design of a dual-band BPF using the first and second resonant modes of a stepped-impedance RR[16]. However, this method fell short in creating two transmission poles in the second passband. In another study[20], two distinct RRs, featuring varying shapes or diameters and utilizing single and two-layer substrates, were appropriately fabricated. In this scenario, the dual pass-bands, each with two poles, were achieved through two different degenerate modes in two separate RRs. Surprisingly, limited research has focused on developing dual-band filters with two transmission poles in both pass-bands using an RR. With this in mind, our investigation delves into the transmission line properties of a plasmonic HMIM waveguide and the dual-band filter characteristics of CRR. In this paper, we present the design and exploration of a CRR for a dual-band BPF application.

HMIM (Ag-SiO_2-Si-SiO_2-Ag) plasmonic waveguide is sandwiched with two metal layers of Ag with an insulator of high and low dielectric slabs of Si and SiO_2, which is illustrated in Fig.1(a). The Ag is used as metal and is defined using Drude model[19], i.e., $\varepsilon=\varepsilon_\infty-\omega_p/\omega^2+j\omega\Gamma$, where $\varepsilon_\infty=1$ is the dielectric constant at infinite angular frequency. $\omega=1.39\times10^{16}$ is plasma frequency and $\omega_p=3.08\times10^{13}$ is damping frequency. The refractive indices of Si and SiO_2 are 1.44 and 3.48[19], respectively. The thicknesses of the HMIM waveguide layers are $t_{Si}=150$ nm, $t_{SiO2}=20$ nm, $t_m=100$ nm and the height of the substrate is 200 nm.

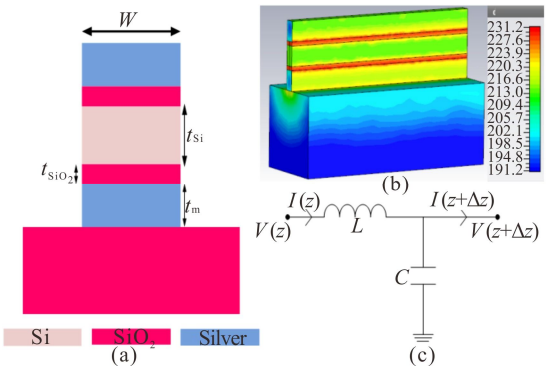

Fig.1 (a) Schematic of HMIM waveguide; (b) Field distribution; (c) Equivalent model

All the simulations are carried out using full wave electromagnetic simulator CST studio suite, as the wave propagation takes place through Ag-SiO_2 interface.

The significant plasmonic modes are due to the metal and dielectric (Ag-SiO_2) interface. The conventional modes are made possible with the Si slab. Both the modes are combined to generate the hybrid modes as required. The HMIM waveguide field distribution is represented in Fig.1(b). The equivalent circuit of the HMIM waveguide is given in Fig.1(c).

The complex propagation constant is given as $\gamma=\alpha+j\beta$. The propagation length ($L_{spp}=1/2\alpha$) is inversely proportional to attenuation constant (α), which deals with scattering and metal absorption losses.

For deep insight into the material properties in response to the corresponding operating wavelength, the wavelength response plots pertaining to characteristic impedance (Z_{PV}), effective refractive index (Real(n_{eff})) and propagation length (L_{spp}) are plotted as represented in Figs.2—4, respectively for varying slot widths (W).

The Z_{PV} of the HMIM slot waveguide increases by decreasing W. The W takes different values form 50 nm to 180 nm with 10 nm interval, and the corresponding impedance drops from 290 Ω to 170 Ω of its peak values. The relation is constant throughout the wavelength range from 1 000 nm to 3 000 nm shown in Fig.2. The variation of Real(n_{eff}) increases as the slot width (W) increases represented in Fig.3. The L_{spp} reported a parabolic growth with wavelength by varying W shown in Fig.4.

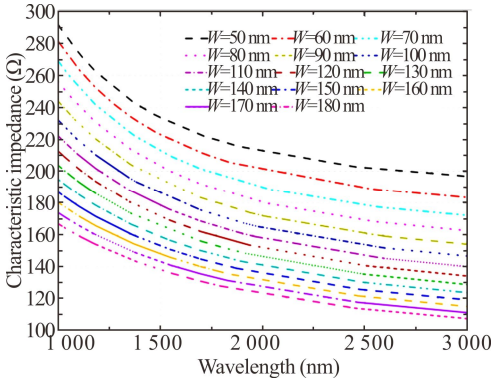

Fig.2 Variation in characteristic impedance with slot width as a function of wavelength

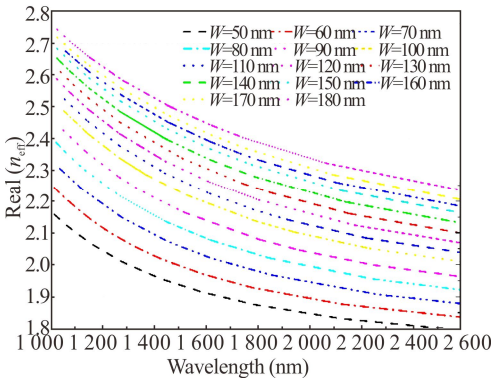

Fig.3 Variation in Real(n_{eff}) with slot width as a function of wavelength

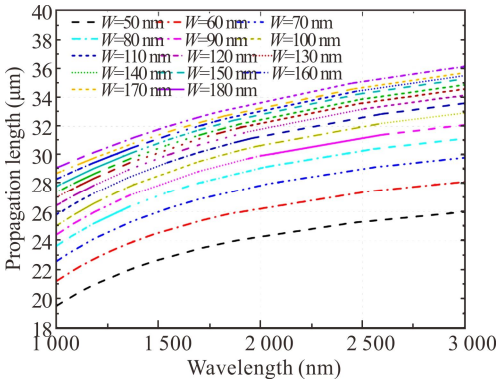

Fig.4 Variation in propagation length with slot width as a function of wavelength

Due to the simplicity and easy designing, RRs are usable in a variety of applications like filters, delay lines or buffers, etc[20-24], which are useful for communication purposes in photonic integrated circuits. The RRs are storing the energy at the resonance, and also they can be used for optical delay lines. The HMIM waveguide-based DR-DB-BPF is sketched in Fig.5. Fig.5 illustrates HMIM waveguide-based DR-DB-BPF consisting of two circular rings with gap g_1 and placed in the middle of the two feed lines. The CRR is placed in close vicinity of a straight HMIM waveguide with a gap g to allow coupling. The characteristics of metals and insulators have been described earlier. The configuration accommodates waves with a wavelength that is a whole number multiple of the guided wavelength and matches the average circumference.

The resonant wavelengths of a CRR are obtained by[23,24]

$$\frac{J_n'\left(kR_{\text{out}}\right)}{J_n'\left(kR_{\text{in}}\right)}-\frac{N_n'\left(kR_{\text{out}}\right)}{N_n'\left(kR_{\text{in}}\right)}=0, \tag{1}$$

where $k=\omega(\varepsilon_0\varepsilon_r\mu_0)^{1/2}$, and $\varepsilon_r=(n_{\text{eff}})^2/\mu_0$ is the relative permittivity. J_n and N_n are the first and the second kinds of Bessel functions of order n. J_n' and N_n' are derivations of the Bessel functions with respect of the argument (kR). Eq.(1) is solved for getting resonant wavelengths of the proposed structure.

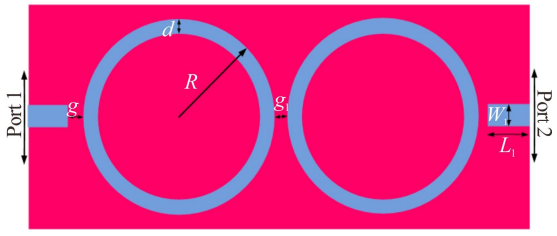

Fig.5 The proposed structure of dual-CRR

The DR-DB-BPF structure consists of two coupled HMIM waveguides as represented in Fig.5, in which the inner radius is denoted by R_{inner} and outer radius by R_{out}. The actual radius (R) of the ring is considered to be the mean value of R_{out} and R_{inner}, i.e., $R=(R_{\text{out}}+R_{\text{inner}})/2$. The optimized length for mean radius (R) is 596 nm. The width W_1 of the coupled HMIM waveguide is 70 nm, length L_1 is 200 nm, and g is the gap between CRR and HMIM waveguide and is 2 nm.

The reflection and transmission coefficients of DR-DB-CRR with respect to the wavelength are represented in Fig.6. The physical dimensions of the proposed structure are W_1=70 nm, L_1=100 nm, R=590 nm, g=2 nm and g_1=2 nm. The overall size of the DR-DB-BPF is 2 790 nm×1 384 nm. The first pass-band occurred at the fundamental frequency of $f_{\text{fundamental}}$=230.6 THz (1 300.5 nm) at the same time as second pass band occurred at the spurious frequency of f_{spurious}=187.4 THz (1 599.74 nm). The energy gets coupled to the DR-DB-CRR at two wavelengths as shown in Fig.7.

The spectral characteristics of extinction ratio (*ER*) (~35 dB), free spectral range (*FSR*) (299.69 nm), full width half maximum (*FWHM*) (78.057 nm at 1 300.5 nm and 112.43 nm at 1 599.74 nm), finesse (3.839 at 1 300.5 nm and 2.665 at 1 599.74 nm), and Q factors (21.987 at 1 300.5 nm and 18.556 at 1 599.74 nm) are observed at the resonant wavelengths.

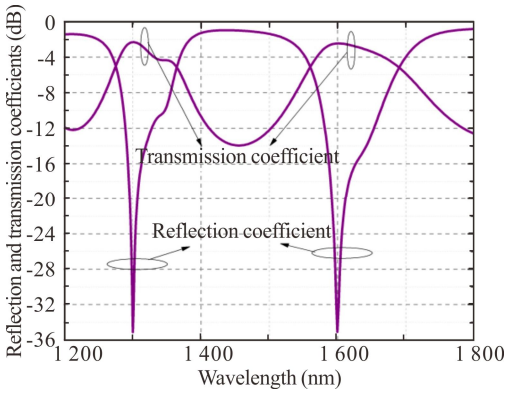

Fig.6 Transmission and reflection coefficients variations with wavelength for the proposed DR-DB-BPF

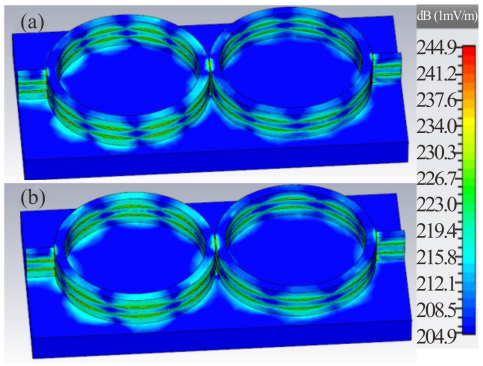

Fig.7 Field distributions at wavelengths of (a) 1 300.5 nm (230.6 THz) and (b) 1 599.74 nm (187.4 THz)

The energy is directly coupled through CRR from the waveguide. The field distributions at the fundamental wavelength of 1 300.5 nm (230.6 THz) and the spurious wavelength of 1 599.74 nm (187.4 THz) are represented

in Fig.7(a) and (b), respectively.

By including another circular ring in the DR-DB-BPF, the design of TR-DB-BPF is proposed. The CRR with radius r (580 nm) connected to HMIM waveguide of width (W_1=60 nm) and length (L_1=200 nm) is represented in Fig.8. The gap between the waveguide and circular ring is g (2 nm) and gap between two rings is g_1 (2 nm). The overall size of the proposed TR-DB-BPF is 3 888 nm×1 310 nm. The HMIM waveguide supports the transverse magnetic (TM) mode of propagation. The reflection and transmission coefficients of TR-DB-CRR with respect to the wavelength are represented in Fig.9.

The first pass-band of TR-DB-BPF occurs at the 236.2 THz (1 269.23 nm) at the same time as second pass-band has occurred at 192 THz (1 561.41 nm). The energy gets coupled to the TR-DB-CRR at two wavelengths shown in Fig.10. The field distributions are mainly concentrated on the metal insulator regions of the HMIM based CRR and the strong energy fields are observed from port 1 to port 2 at the resonating wavelengths.

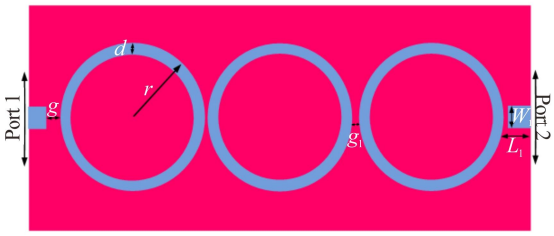

Fig.8 Triple-ring CRR

The proposed TR-DB-CRR have ~22.5 dB of *ER*, 292.18 nm of *FSR*, 42.751 nm and 59.58 nm of *FWHM* at 1 269.23 nm and 1 561.41 nm, respectively, finesse (6.834 at 1 269.23 nm and 4.903 at 1 561.41 nm) and Q factors (37.57 at 1 269.23 nm and 55.60 at 1 561.41 nm) observed at the resonant wavelengths. The reflection and transmission coefficients of the TR-DB-BPF at fundamental wavelength are 236.2 THz (1 269.23 nm) which is equivalent to $3\lambda g/2$ as shown in Fig.9.

The field distributions at wavelengths of 1 269.23 nm (236.2 THz) and 1 561.41 nm (192 THz) are represented in Fig.10. The proposed DR-DB-BPF and TR-DB-BPF are useful for developing EPICs. These proposed silicon waveguides and BPFs are fabricated using E-beam or optical lithography techniques and CMOS manufacturing process.

The HMIM waveguide basic characteristics have been studied and numerically analyzed. The reflection and transmission coefficients of HMIM slot waveguide based CRR along with the resonant behavior of RR have been studied and numerically investigated. DB characteristics of RR have been found and useful in the design of DB EPICs. The DR-DB-BPF is operated at 1 300.5 nm and 1 599.74 nm, respectively. The spectral analysis parameters *ER*, *FSR*, *FWHM*, finesse and Q-factor of DR-DB-BPF are 35 dB, 299.69 nm, 78.057—112.43 nm,

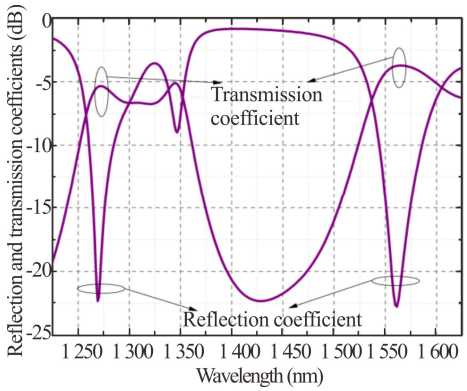

Fig.9 Transmission and reflection coefficients variations with wavelength for the proposed TR-DB-BPF

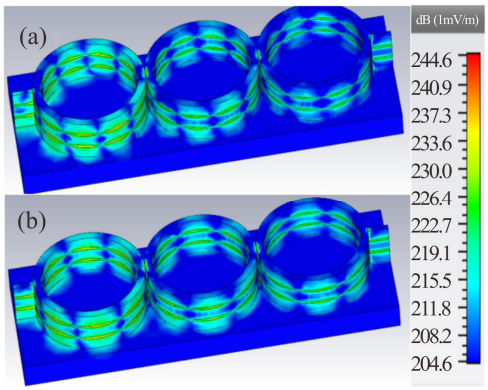

Fig.10 Field distributions at wavelengths of (a) 1 269.23 nm (236.2 THz) and (b) 1 561.41 nm (192 THz)

3.84—2.64 and 21.9—18.556, respectively. The proposed TR-DB-BPF are operated at 1 260 nm and 1 560 nm, respectively, and have 25.6 dB, 279.25 nm, 22—38 nm, 7—12 and 40—54 of *ER*, *FSR*, *FWHM*, finesse and Q-factor, respectively. The HMIM waveguide structures can be further extended to design several other plasmonic components, such as diplexers, power dividers/splitters and couplers.

Ethics declarations

Conflicts of interest

The authors declare no conflict of interest.

References

[1] ZHU J, ZHU T, JIA H, et al. Intuitive analysis of subwavelength plasmonic waveguide[J]. Journal of lightwave technology, 2019, 37(4): 1345-1351.

[2] ZHANG Z. Silicon-based photonic devices: design, fabrication and characterization[J]. Atom & molecular physics & optics, 2008.

[3] DU W, WANG T, CHU H S, et al. On-chip molecular electronics plasmon sources based on self-assembled monolayer tunnel junctions[J]. Nature photonics, 2016, 10: 274-280.

[4] LIU Y, ZHANG J, LIU H, et al. Electrically driven monolithic subwavelength plasmonic interconnect circuits[J]. Science advances, 2017, 3(10): 1-8.

[5] PATEL V, SHARMA P, KUMAR V D. Efficient coupling from dielectric to hybrid plasmonic waveguide using curved taper[J]. IEEE photonics technology letters, 2019, 31(4): 323-326.

[6] LIU Y, ZHANG J, PENG L M. Three-dimensional integration of plasmonics and nanoelectronics[J]. Nature electronics, 2018, 1(12): 644-651.

[7] SHARMA P, DINESH K V. Hybrid metal insulator metal plasmonic waveguide and ring resonator[C]//Proceedings of 2016 OptoElectronics and Communications Conference, July 3-7, 2016, Niigata, Japan. New York: IEEE, 2016: 1-3.

[8] KRITARTH S, DINESH K V. Investigation of light coupling between HMIM and HIMI plasmonic waveguides[J]. Optical and quantum electronics, 2021, 53: 225.

[9] TIAN J, YANG R, SONG L, et al. Optical properties of a Y-splitter based on hybrid multilayer plasmonic waveguide[J]. IEEE journal of quantum electronics, 2014, 50(11): 898-903.

[10] DU C H, CHIOU Y P. Vertical directional couplers with ultra-short coupling length based on hybrid plasmonic waveguides[J]. Journal of lightwave technology, 2014, 32(11): 2065-2071.

[11] SHARMA P, KUMAR V D. Investigation of multilayer planar hybrid plasmonic waveguide and bends[J]. Electronics letters, 2016, 52(9): 732-734.

[12] SHARMA P, KUMAR V D. All optical logic gates using hybrid metal insulator metal plasmonic waveguide[J]. IEEE photonics technology letters, 2018, 30(10): 959-962.

[13] SEHAM A E, NIHAL F F A, HAMDI A E M, et al. Tunable multi-channels bandpass InGaAsP plasmonic filter using coupled arrow shape cavities[J]. Photonics, 2022, 9(10): 1-11.

[14] CASPERS J N, MOJAHEDI M. Measurement of a compact colorless 3 dB hybrid plasmonic directional coupler[J]. Optics letters, 2014, 39(11): 3262-3265.

[15] MOHAMMAD S, ALI P, REZA G B. Hybrid MIM plasmonic waveguide by triangular grooves[J]. Optik, 2023, 273: 170441.

[16] KUMAR B S, SRIDHAR M. Design and analysis of HMIM waveguide based dual band BPF for nanoscale applications[J]. Design engineering, 2021: 1025-1032.

[17] WOLFF I, KNOPPIK N. Microstrip ring resonator and dispersion measurement on microstrip lines[J]. Electronics letters, 1971, 7(26): 779-781.

[18] PINTU K, DHARMENDRA K S, RAKESH R. Optical performance of hybrid dielectric loaded plasmonic waveguide using PTFE for nano-scale light confinement[J]. Optoelectronics letters, 2020, 16(7): 284-289.

[19] MAIER S A. Plasmonics: fundamentals and applications[M]. 1st ed. Berlin, Heidelberg: Springer, 2007.

[20] SHIVA K, MOHAMMAD D, PEJMAN R. Design of single mode plasmonic bandpass filter using a hexagonal resonator coupled to graded-stub waveguides[J]. Plasmonics, 2019, 14: 6850.

[21] KHATAB H M, AREED N F F, EL-MIKATI H A, et al. Efficient plasmonic line-up filter for sensing applications[J]. Optical quantum electronics, 2021, 54: 47.

[22] SURENDRA K B, SRIDHAR M, SANTHOSH C H, et al. Terahertz analysis of a highly sensitive MIM-SRR_TiO_2 nanostructure for bio-sensor applications with the FDTD method[J]. Journal of optical society America B, 2022, 39(1): 223-229.

[23] THIRUPATHAIAH K, RAO L K, RAVI B. Nanoplasmonic directional coupler using asymmetric parallel coupled MIM waveguides[J]. IEEE photonics technology letters, 2022, 34(8): 401-404.

[24] YU Y, LIU B, YANG F, et al. Design and fabrication of room temperature electrically pumped ZnO nanowire hybrid plasmonic lasers[J]. IEEE photonics technology letters, 2023, 35(16): 899-902.